THE AMERICAN SOCIETY OF MECHANICAL ENGINEERS
345 E. 47 St., New York, N.Y. 10017

86-GT-304

Numerical Investigation of Unsteady Subsonic Compressible Flows Through an Oscillating Cascade

T. H. FRANSSON
Ecole Polytechnique Fédérale de Lausanne
Lausanne, Switzerland

M. PANDOLFI
Politecnico di Torino, Turin, Italy

ABSTRACT

A method for solving numerically the fully time-dependent two-dimensional Euler equations, applied to unsteady subsonic flow through vibrating turbomachine cascades with thin blades, is developed. The blades are assumed to vibrate at a constant interblade phase angle and the computed region is reduced to one blade passage, with the implementation of the interblade phase angle as a periodicity condition. The reliability of the method is validated by comparing it with an analytical flat plate theory, and the importance of radiative inlet and outlet boundary conditions for unsteady flow calculations is shown in an example.
The method can be used to compute the aerodynamic force and damping coefficients acting on the blades and to investigate the propagation of unsteady disturbances through a cascade in flutter conditions.

NOMENCLATURE

A	amplitude (-)
b(z,t)	lower time-dependent boundary (-) (Fig. 2)
c	chord (m)
c(z,t)	upper time-dependent boundary (-) (Fig. 2)
$C_L(t)$	lift coefficient (-)
C_L	amplitude of C_L for harmonic motion (-)
f	function
k	reduced frequency, $k=\omega c/2q_{-\infty}$ (-)
L	grid number in Z direction (-)
l_r	reference length = chord (m)
M	grid number in Y direction (-)
M	Mach number (-)
p	pressure (N/m^2, -)
q	velocity (m/s, -)
R	gas constant, R=287 $m^2/(s^2k)$ for air
s	entropy (m^2/s^2K)
t	time (s,-)
T	temperature (K)
T	dimensionless time (-)
T_0	period of a cycle (-)
v	velocity in y direction (m/s,-)
w	velocity in z direction (m/s,-)
y	circumference coordinate in the physical plane (-)
Y	circumference coordinate in computational plane of reference (-)
z	axial coordinate in the physical plane (-)
Z	axial coordinate in the computational frame of reference (-)
$\Delta c_p(z,t)$	blade surface pressure difference coefficient = $\frac{1}{A}\frac{p(z,t)^{ls}-p(z,t)^{us}}{\bar{p}_{t-\infty}-\bar{p}_{-\infty}}$ (-)
γ	stagger angle (deg)
$\Delta c_p(z)$	amplitude of $\Delta c_p(z,t)$ at harmonic motion (-)
ρ	density (kg/m^3)
σ	interblade phase angle (deg)
τ	steady state pitch-to-chord ratio (-)
Φ_L	phase lead of lift coefficient towards harmonic motion (deg)
$\Phi_{\Delta p}(z)$	phase lead of blade surface pressure difference coefficient towards harmonic motion (deg)

Presented at the International Gas Turbine Conference and Exhibit
Dusseldorf, West Germany—June 8-12, 1986

ω	circular frequency of blade vibration (deg)

Subscripts and Superscripts

r	reference values
$-\infty$	values at infinity upstream
$+\infty$	values at infinity downstream
Y	derivatives in Y direction
Z	derivatives in Z direction
$\tilde{}$	velocity components tangential and normal to the contour adapted grid
$\bar{}$	time averaged values
ls	lower surface
us	upper surface

INTRODUCTION

The excitation of blade vibrations in turbomachines may be either forced or self-sustaining. In the first type (forced vibrations), phenomena such as:

- multiples of rotor frequencies
- inlet distortions in temperature, velocity and flow direction
- stator-rotor interactions

can be found.

The second type (self-excited blade vibrations or blade flutter) is produced by the interaction of a blade movement and the time-dependent aerodynamic forces resulting from it.

In a turbomachine, flow phenomena from both these groups interfere with each other and create a complicated unsteady flow pattern through the stages. This pattern cannot be predicted by present theoretical methods, wherefore several idealizations of the time-dependent flow are normally made.

As regards self-excited blade vibrations, different flutter regions related to the flow conditions in the engine have been identified throughout the years, both in compressors and in turbines. Because of the high demands made on modern jet engines, most of the flutter problems reported have occurred in the fan stages of these machines. However, flutter phenomena have recently also become of practical interest in transonic steam and gas turbines, especially at high back pressures. Under these operating conditions, the flow in the blade passage is presumably partially or fully stalled.

Some of the possible types of blade flutter are shown schematically in Figure 1, which gives a typical modern compressor chart.

Depending upon the flow conditions, the different flutter types in Figure 1 may be characterized (see for example /1-3/) as:

1. Subsonic/transonic positive incidence stall flutter, in which the compressor operates near the surge line either at part speed or near design speed. Although the term "stalled" is generally used, it is not established that the flow in this flutter region is always separated over the whole blade.
2. Negative incidence transonic choke flutter, at part speed. This type of flutter may appear when the flow in a compressor accelerates through sonic transition. This flutter region is probably associated with local blade separations and unsteady shock waves.
3. Supersonic positive incidence stall flutter. The flow is supersonic at the outer region of the blade and the stage operates near the surge limit. The flow probably has strong in-passage shocks.
4. Unstalled supersonic flutter, at full speed and with attached flow. This can occur at design point and at higher or lower pressure ratios and may limit high speed operations.
5. Supersonic flutter (type "A100"). This type of blade flutter has been found to appear suddenly above a certain pressure ratio, below which there is no flutter. Increased loading may shift this critical pressure ratio.

All the above-mentioned flutter limits are of wide practical interest and several investigations, both experimental and theoretical, have been done on each region.

Theoretical models exist presently for the prediction of unstalled self-excited blade vibrations (regions 6, 7 and 8 in Fig. 1), but most prediction methods for partially or fully stalled flow are closely linked to extensive experimental data to produce semi-empirical models.

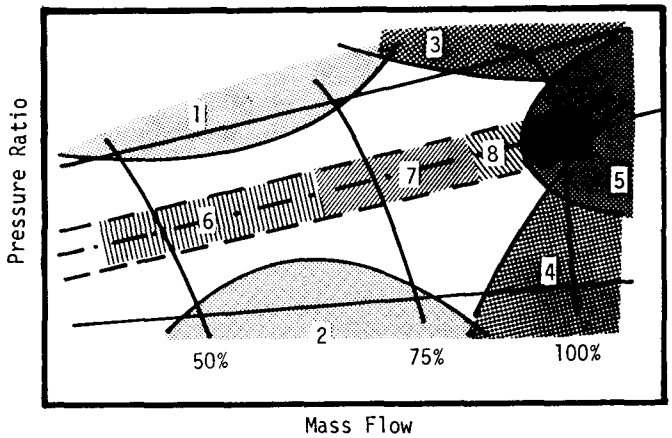

Fields 6,7 and 8: Fields of application of present fully theoretical subsonic (6), transonic (7) and supersonic (8) prediction models.

Fig. 1. Different flutter types in axial compressors (See for example /1/).

Several of the existing theoretical prediction models for unstalled flow agree well with the measured aeroelastic forces acting on vibrating blades (see for example /4-10/). However, as industry's main interest is to compute the unsteady blade forces as quickly and cheaply as possible in order to avoid blade failures, only a very limited number of methods also take into consideration the non-linear unsteady flow in the blade passage /8,9/ although an understanding of how disturbances are propagated from one blade to another is essential to the fundamental comprehension of aeroelastic phenomena in blade rows.

It is the aim of the present study to present a fully unsteady numerical method for predicting both the aeroelastic blade forces and the unsteady flow through vibrating cascades, and thus contribute to the comprehension of unsteady physical flow phenomena in turbomachines.

In its present form the analysis developed is restricted to inviscid subsonic flow through two-dimensional thin compressor cascades (region 6 in Fig. 1), but as the method presented has proved useful it can be extended to thick, cambered turbine blades with transonic flow and oscillating shock waves (region 7 in Fig. 1).

GOVERNING EQUATIONS AND NUMERICAL METHOD OF SOLUTION.

We consider the full Euler equations for describing two dimensional unsteady, inviscid, compressible flow through a cascade , written in the non-conservative form and expressing the physical principles of continuity of mass, equilibrium of forces and conservation of energy /11/:

$$\text{Continuity eq.:} \quad \frac{\partial \rho}{\partial t} + \operatorname{div}(\rho \vec{q}) = 0$$

$$\text{Momentum eq.:} \quad \frac{\partial t}{Dt} + \frac{1}{\rho} \vec{g}\operatorname{grad}(p) = 0 \qquad (1)$$

$$\text{Energy eq.} : \quad \frac{Ds}{Dt} = 0$$

where p, ρ, $\vec{q}$, s denote the pressure, density, velocity vector and entropy, respectively. Time is denoted by t and

$$\frac{Df}{Dt} = \frac{\partial f}{\partial t} + \vec{q}\ \operatorname{grad}(f)$$

where f is an arbitrary function. In what follows, the entropy equation will be omitted,as the upstream entropy is considered to be constant for all the cases dealt with in this article.

This non-linear system of partial differential equations can be solved by a numerical method based on a finite difference approximation. For the model used in the present study, Eq. (1) is written in a non-dimensionalized form as (see /12/ for details):

$$\text{Continuity eq.:} \quad \frac{D(\ln p)}{Dt} + \rho \operatorname{div}(\vec{q}) = 0$$

$$\text{Momentum eq.:} \quad \frac{D\vec{q}}{Dt} + \frac{p}{\rho} \operatorname{grad}(\ln p) = 0 \qquad (2)$$

where the physical variables are normalized with the reference values: pressure p_r, length l_r, time $t_r = l_r/q_r$, temperature T_r, and velocity $q_r = \sqrt{RT_r}$.

The method used for this work is equivalent to steady-state time-dependent Euler solvers as long as the boundary conditions (blade positions, flow variables at inlet and outlet reference planes) are maintained constant in time. If a blade movement is introduced, the solution to the unsteady flow through the vibrating cascade will be found.

Before applying the finite difference approximation to equations (2) these are mapped from the physical plane into a rectangular computational plane of reference (Fig. 2) with the normalized transformation (z,y,t)→(Z,Y,T):[1]

$$Z(z) = \frac{Z - Z_1}{Z_2 - Z_1}$$

$$Y(z,t) = \frac{y - b(z,t)}{c(z,t) - b(z,t)} \qquad (3)$$

$$T = t$$

where the boundaries b and c (representing the pitch) are allowed to move in time. Equation system (2) thus becomes:

$$(\ln p)_T = f_1 + f_4$$

$$\tilde{w}_T = f_2 + f_5 \qquad (4)$$

$$\tilde{v}_T = f_3 + f_6$$

[1] This transformation is a of general nature. However, it is not suitable for blades with thick leading edges as the change in grid direction is not continuous in the leading edge plane for these "H-grids".

where $\tilde{w}$ and $\tilde{v}$ are velocity components, along a constant Y, and normal to it, respectively. The functions f_1- f_3 depend on the spatial derivatives of the primitive variables ln(p), $\tilde{w}$,$\tilde{v}$ and the functions f_4-f_6 depend on transformation (3) and contain geometrical derivatives only. (The detailed development of eq. system (4) can be found in /12/).

The second stage of the solution procedure involves discretizing the partial differential equation system (4), which is written in the computational frame of reference, according to a finite difference approximation. For the present application it was decided to use the standard explicit second order (in time and space) predictor-corrector MacCormack scheme /13/, to approximate the spatial differences f_Y and f_Z in eq. (4) and to integrate numerically the three primitive variables ln(p), $\tilde{w}$ and $\tilde{v}$ in time.

Finally, the appropriate boundary conditions should be imposed according to the physical requirements of the unsteady flow. The method used in the present work is Moretti and de Neff's post correction technique/14/.

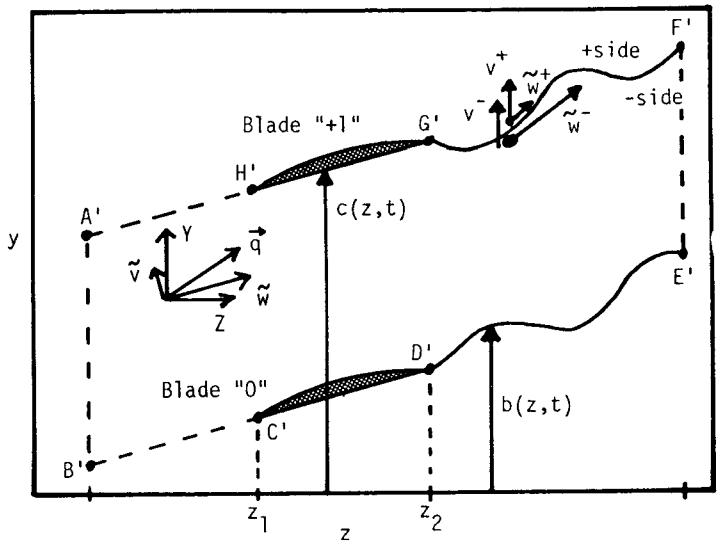

a. Physical plane

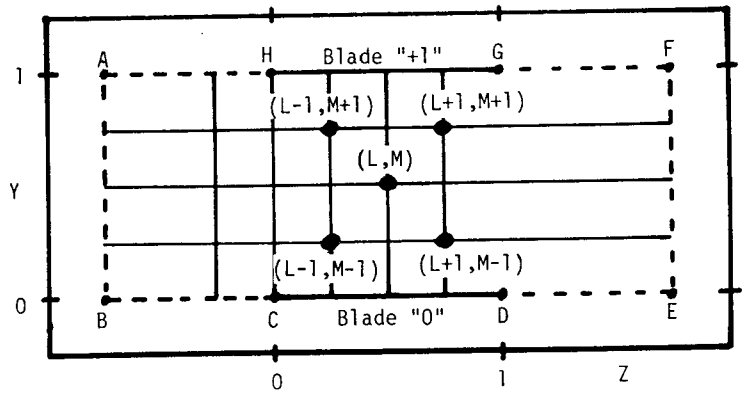

b. Computational plane of reference

Fig. 2. Physical and computational planes of reference.

In this technique the numerical treatment of computational points located on boundaries is in two steps. First, the computation is done using, for the approximation of derivatives at the boundaries, values from interior points only. In this preliminary computation the boundary condition is not yet imposed. Therefore, the flow variables calculated are not correct. However, considering the hyperbolic or wave-like nature of the Euler equations, the Rieman variables (a specific combination of pressure and velocity component) carried on characteristics impinging upon the boundary are expected to be correct /14/.The values of the primitive flow variables computed so far thus have to be changed by imposing the required boundary condition, while maintaining the value of the Rieman variable just computed.

This updating is performed as the final logic at every time step.

The following boundary conditions have been used:

At the inflow boundary two boundary conditions have to be provided. In the present work these boundary conditions were applied in two different ways. The first is that used in most Euler solvers, i.e. the specification of stagnation temperature (or stagnation pressure) and flow direction at the inlet surface. This method of treating the boundary introduces reflections of the unsteady disturbances impinging upon the boundary from inside the flow field. These reflections may distort the results from the calculation with vibrating blades (and may also make the convergence for reaching a steady state solution somewhat slower). A second way to treat the flow at the boundary could be to simulate the so-called "radiative" boundary condition. The basic idea behind this boundary condition is that in a cascade, in contrast to an isolated airfoil where disturbances propagated away from the airfoil diminish in strength with the radial distance from the profile, the flow is bounded up- and downstream. The disturbances will thus not decrease in strength. However, if the flow upstream of the cascade is undisturbed from the left, the disturbances running to the left will be simple wave fronts. If, after a certain distance, these wave fronts are straight, it is expected that the reflections from an upstream computational boundary can be reduced. In contrast to the first technique, the boundary conditions are not imposed at the inlet, but it is considered instead that a right running characteristic (coming from upstream infinity) carries information in an isentropic way from upstream infinity to the inlet, and into the flow field. The boundary condition imposed at the inlet is therefore the right running Rieman variable (which

corresponds to specifying total and static pressure as well as flow direction at upstream infinity). This way of treating the boundary has been useful for the cases considered in the present work (rather thin profiles with small camber).

In subsonic flow one boundary condition has to be provided at the outlet boundary. As in the case of the inlet boundary, two different techniques were used. The first specifies the outlet static pressure as a constant value.

The second uses a similar technique as at the inlet while imposing the left running Rieman variable as a boundary condition.

At the solid walls (blades) a flow tangency condition is used.

The upstream periodic boundary conditions are satisfied by treating points on them as interior points and using values of flow properties outside the computed region. These are taken to be equal to those of one blade pitch and the defined interblade phase angle within the region. This means that, for calculation of the flow variables on for example the upper upstream periodicity line (AH in Fig. 2), the value of the flow variables at any point above blade "+1" at time t_1 are made to correspond to the value at the point above blade "0" at time t_2. Thus:

$$f_{MCP,L}^{t=t1} = f_{3,L}^{t=t2}, \text{ where } t_2=t_1+\sigma/\omega=t_1+\sigma T_0/2\pi \quad (5)$$

This periodicity condition is updated during every vibration cycle.

Since, in unsteady flow, vorticities leave the trailing edge and are convected downstream, the downstream slipstream has to be treated as a discontinuity /15/. On each side of this vorticity sheet the tangential velocity component ($\tilde{w}$) may be different, whereas the normal velocity component ($\tilde{v}$) and the static pressure are the same on both sides (Fig. 2a). To simulate this physical phenomenon of vorticity convection, a flexible slipstream is introduced and allowed to move in time and space as part of the calculation. No explicit boundary conditions are imposed, but the physical conditions of no pressure jump and normal velocity are implicitly introduced using the post correction technique /15/. This way of treating the slipstream explicitly has proved to be accurate in relating the amount of vorticity shed by the blading and the instantaneous lift on it /15/. This feature seems to be extremely important in describing the unsteady flow around blades in cascades.

As for the upstream periodicity line, care must be taken to use values of the flow variables which take the pre-defined interblade phase angle into account.

EXAMPLES OF APPLICATIONS

Steady State Bumpflow: As an example of a steady state solution the flow through a channel with a 10% thick bump on the lower wall is given. Agreement between the present results and the ones presented by Ni /16/ is good (Fig. 3).

Validation of Periodic Boundary Conditions: In the case of a 180° interblade phase angle in the movement between adjacent blades, a straightforward verification of the periodicity assumption as presented above can be performed in a fairly simple manner.

Between two blades vibrating in normal to chord bending and in phase with each other (Fig. 4, blades "0" and "+2"), one intermediate fixed blade is introduced (blade "+1"). This movement of the cascade corresponds to a case of a 180° interblade phase angle as far as the phase angle of the responding flow variables is concerned. Obviously, no conclusion about the amplitude of the result can be drawn from this investigation.

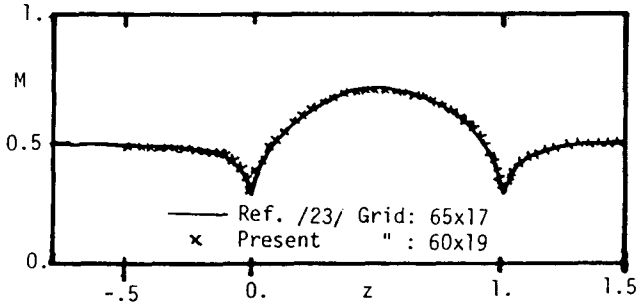

Fig. 3. Mach number distribution for bump-flow.

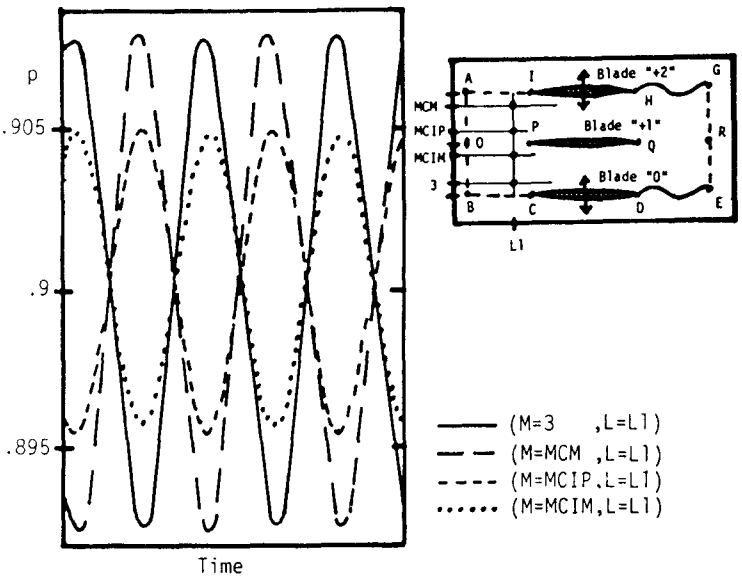

Fig. 4. Pressure fluctuations in time with an intermediate blade.

At all the boundaries AOBCDERGHIA the boundary conditions given earlier for zero interblade phase angle are used. At the intermediate blade no boundary conditions are imposed upstream or downstream of the blade (lines OP and OR respectively). Instead, the values of the flow variables on these lines are the results of calculations of interior points only.

When blades "0" and "+2" move upwards, the relative movement of blade "+1" towards blade "0" is downwards, i.e. both blades create an overpressure in the blade passage between them (OBCDERQPO); it is therefore expected that the response of the flow variables on lines M=MCIM and M=3 will be identical in relation to the phase angle. Similarly, the phase angle on lines M=MCIP and M=MCM should also be identical.

In Fig. 4a comparison of the fluctuating pressures on lines M=3, M=MCIM, M=MCIP and M=MCM is given for an upstream point (L=L1). It should be noted that:

- The pressure responses on lines M=3 and M=MCM have the same amplitude and are 180° out of phase in relation to each other. This is the expected result as blades "0" and "+2" move in phase.
- The pressures on lines M=MCIM and M=MCIP also show the same amplitude and are 180° out of phase. This is correct as the relative motion of blade "+1" towards blades "0" and "+2" creates an overpressure on one side and an underpressure on the other side of the blade.
- The pressures on lines M=3 and M=MCIM are in phase as, in relation to each other, the blades "0" and "+1" have an identical motion. However, the amplitude of the pressures on line M=MCIM is lower than that of the ones on line M=3 as blade "+1" is fixed in the absolute frame of reference, while blade "0" is moving.
- Similarly, the pressures on lines M=MCIP and M=MCM are in phase.
- The pressures on lines M=3 and M=MCIP are 180° out of phase. This phase shift corresponds exactly to the phase angle in the relative blade movement of blades "0" and "+1". Therefore it can be seen that, if the values on line M=3 are used as a boundary condition for line M=MCIP, a phase shift of half a cycle has to be introduced, i.e.:

$$t_2=t_1+T_0/2=t_1+\sigma T_0/2\pi \quad \text{as } \sigma=\pi\ (=180^0)$$

which is in agreement with eq. (5).

The proposed assumption for periodicity conditions at non-zero interblade phase angles is thus validated for $\sigma=180°$.

Comparison with an Analytical Linearized Theory for Different Interblade Phase Angles: Further to the validation of the assumed boundary conditions as discussed in the previous chapter, comparisons have been made with the linearized subsonic analytical flat plate theory by Smith and Whitehead /4/.

The validation is done here by comparing the unsteady pressure difference coefficient along the blade ($\Delta c_p(z)$, $\Phi_{\Delta p}(z)$) according to the flat plate theory with the calculations of the present model on a 4% thick Double Circular Arc profile, at a moderate inlet Mach number ($M_{-\infty}$ = 0.4) and at different stagger angles, reduced frequencies and interblade phase angles. The trend of the aerodynamic lift coefficient (c_L, Φ_L) is also given in some cases.

In Fig. 5 the aerodynamic lift coefficient is compared for a 90° stagger angle and a high pitch-to-chord ratio (τ = 5.0), at a high reduced frequency (based on half chord) of k = 1.4. This case can be considered as close to an isolated blade case. It is thus expected that both the amplitude and phase angle of the lift coefficient remain almost constant at different interblade phase angles.

This is concluded to be the case for both methods, although the analytical theory shows a big change at a 0° interblade phase angle. This is due to the closeness to the acoustic resonance (/5/), which for the case calculated is situated at a 10° interblade phase angle. Apart from this resonance, the results obtained from the two methods agree well.

In Fig. 6 the blade surface pressure difference coefficient and aerodynamic lift coefficient are given for a case with a pitch-to-chord ratio τ = 1.0.

Fig. 6b shows good agreement for the pressure difference coefficient between the two methods for σ = 0°. Oscillations close to the leading edge for the present method appear because the blades have sharp leading edges and because no artificial damping terms are used in the calculation to smooth out these over- and under-

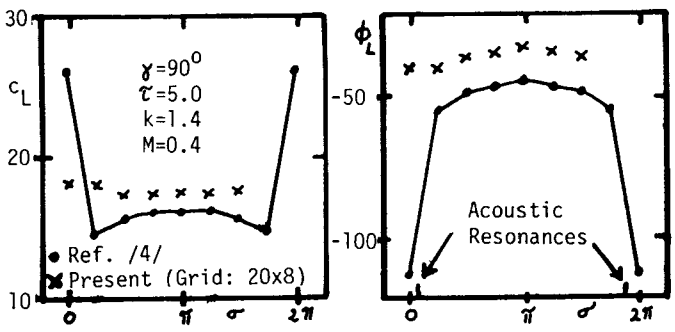

Fig. 5. Aerodynamic lift coefficient.

shoots. In addition, in the results presented, only 12 grid points were used on the blade surfaces.[2]

Agreement between the two methods is however not so good at interblade phase angles of 90° and 180° (Fig. 6b). This is because the analytical theory predicts a constant lift coefficient for all interblade phase angles between the acoustic resonances at σ = 70° and σ = 290° (i.e. in the region of subresonant blade motion according to the linear theory, see /5/) for this high reduced frequency (Fig. 6a). The present method predicts instead an increase in lift coefficient between σ= 0° and σ= 180°, which agrees well with the lift distribution at a lower reduced frequency k= 0.35 (Fig. 7a). At this lower reduced frequency, the unsteady blade surface pressure difference distribution compares well in both methods for all interblade phase angles (Fig. 7b). Oscillations, both in amplitude and phase, at the leading edge region are again noticeable.

In Fig. 8 results are once more presented for k= 1.4, but now at a stagger angle of γ= 60°. Again, a certain difference between the two methods is noted in the

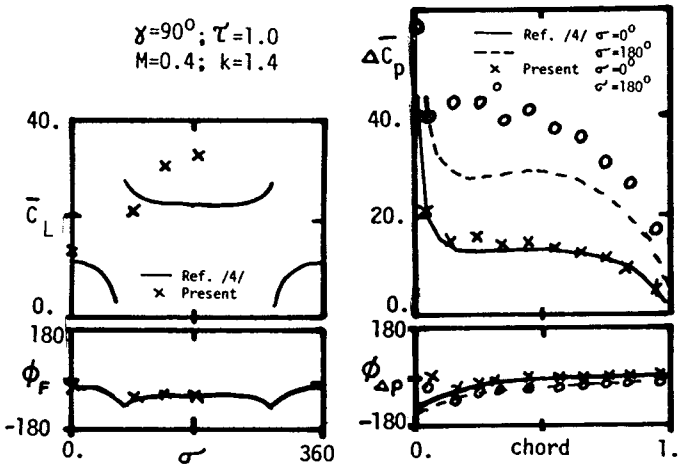

Fig. 6. Blade surface pressure difference and aerodynamic lift coefficients.

[2] The inaccuracy in overall values (for example c_L) due to these numerical oscillations may be reduced (but not completely eliminated) by introducing an artificial damping, and increasing the number of points in the leading edge region. However this has not been done since the main objective is to investigate the propagation of disturbances in the blade passage with a reasonable computer time, and not to use artificial damping devices to give smoothed results. The only way to get rid of these oscillations completely is to use a body-fitted coordinate system (O- or C-grid, and not an H-grid as in the present study) which gives good resolution around rounded leading edges.

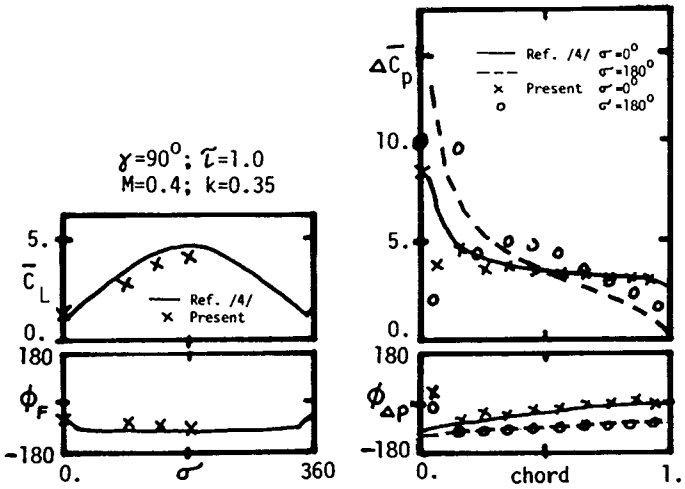

Fig. 7. Blade surface pressure difference and aerodynamic lift coefficients.

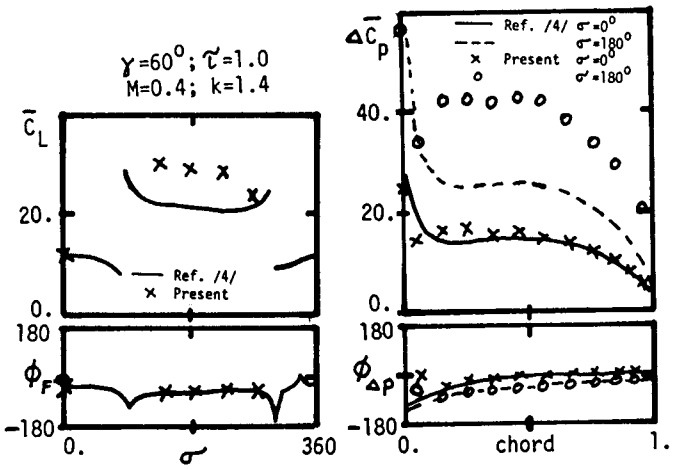

Fig. 8. Blade surface pressure difference and aerodynamic lift coefficients.

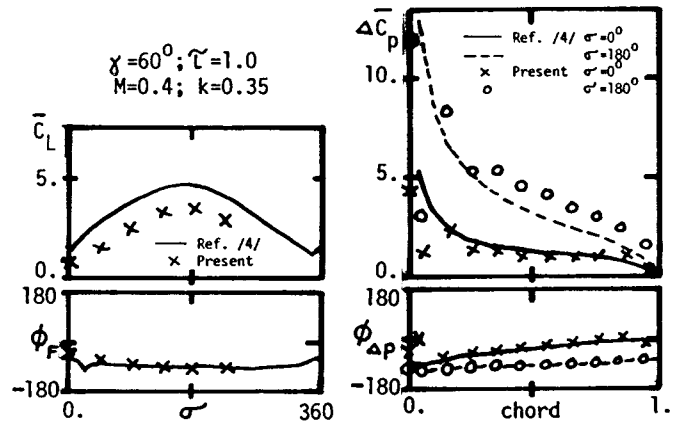

Fig. 9. Blade surface pressure difference and aerodynamic lift coefficients.

aerodynamic lift coefficient between the acoustic resonances σ= 85° and σ = 305° (i.e. in the subresonant region of blade motion, Fig. 8a).
As in the case of a 90° stagger angle, the results at a 0° interblade phase angle agree well (Fig. 8b), but there are some differences in the blade surface pressure difference coefficient in the region between the acoustic resonances.
Also for the cascade with a 60° stagger angle the results of the two methods correspond better when the plateau in the aerodynamic lift coefficient is not predicted by the analytical theory. This is shown in Fig. 9, where results for γ = 60° and k = 0.35 are given. The trend of the aerodynamic lift coefficient is similar for both programs (Fig. 9a), and the detailed blade surface pressure difference coefficients agree well for all interblade phase angles (Fig.9b)[3].
From these verifications it can be concluded that the proposed method of treating the periodicity conditions at non-zero interblade phase angles is reliable for the present method.

Reflective and Radiative Boundary Conditions:

As it is known from linearized theories, the inlet and outlet boundary conditions may significantly influence the unsteady flow through a vibrating cascade. It is thus of importance to, for this new application with a numerical solver, establish the eventual influence of these boundaries.
Such investigations are important for two main reasons:

- If the time-dependent technique aims at a steady solution it is normally of interest to obtain this result as fast as possible. However, care must be taken to simulate the same physical phenomenon. In most cases of stationary flow, the same solution for radiative and reflective boundary conditions will be obtained.
- This is however not always the case during an unsteady flow calculation. Here different boundary conditions simulate separate physical phenomena, and it is not expected that the resulting unsteady flow should be the same for radiative and reflective boundary conditions.

In what follows, two conditions for treating the inlet boundary are presented. The first technique is the one which is usually used for Euler solvers. Here, the incoming flow is considered as coming from an infinitely large capacity with prescribed stagnation pressure. The discharge from the capacity into the physical region of interest is obtained by imaging an infinite number of small nozzles which direct the flow in the desired direction (Fig. 10). As stipulated earlier, the two boundary conditions to be specified at the inlet are stagnation pressure and flow direction.
In the second technique, the inlet and outlet boundaries are instead simulated so as to reduce the reflection. This is done by imaging an infinitely long distance with undisturbed right running characteristics upstream of the inlet (Fig. 10). The left running disturbances are thus simple waves, which are washed out through the boundary with a smaller reflection than in the first technique.
An example of a steady state calculation shows that the convergence time is significantly reduced if the second technique is used (Fig. 11). Convergence is reached after approximately 1/3 of the iterations for the first technique[4].

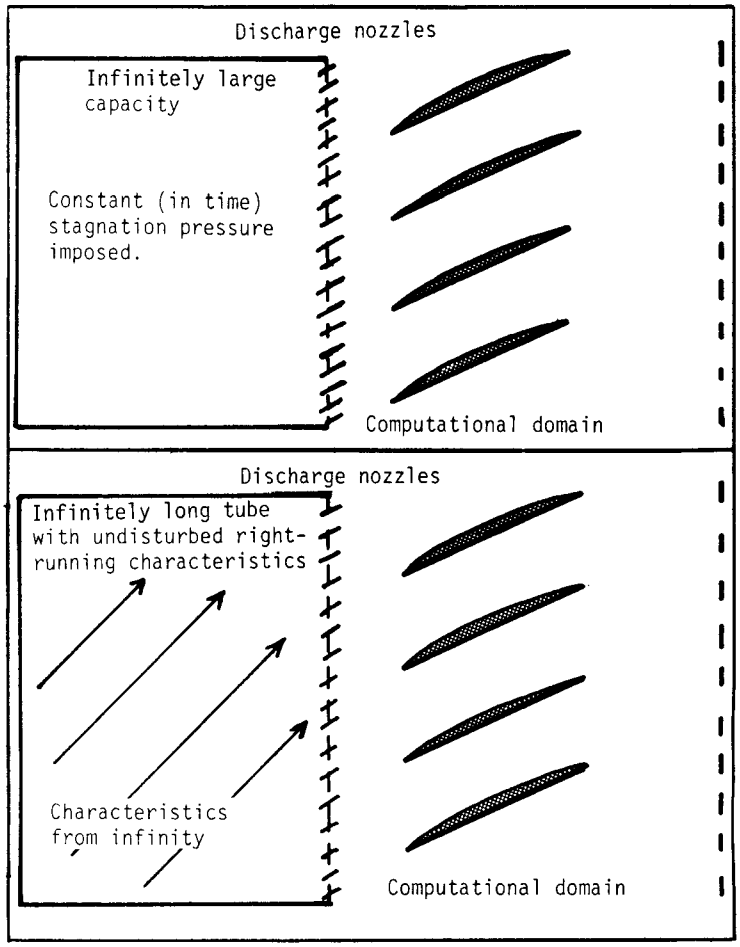

Fig. 10. Physical interpretation of radiative and capacity boundary conditions.

[3] In this context it is of interest to note that one of the conclusions of the project "Aeroelasticity in Turbomachine-Cascades" /10/ was that at high reduced frequencies (k=1.0 in that investigation), fairly large discrepancies between different theories may appear.

[4] If a radiative condition is imposed at the outlet also, the convergence is even faster.

The reason for this change in convergence rate is found at the boundaries. In the first case (stagnation pressure and flow angle prescribed at the inlet, static pressure kept constant at the outlet) the pressure perturbations created in the flow field during the transient are, to a very large extent, reflected back into the cascade at the inlet and outlet boundaries. This can be concluded from Fig. 12a, where the behaviour of the pressure in the inlet region is represented at different time steps.

It should be noted that as the time increases the pressure amplitude peak approaches the inlet boundary. However, close to the inlet (L<3) the amplitude of the pressure waves propagating towards the inlet decreases. This behaviour is typical when a disturbance wave is reflected at the boundary, see Fig. 12b. Here the lines of constant pressure along "L" are represented in time. As the time increases, the isobars first move towards the inlet, but are then turned (reflected) back into the flow field.

In contrast to this reflection, the same diagrams are represented in the case where the "radiative" boundary condition is employed at the inlet. Note (Fig. 12c-d) that the pressure waves created at the blades during the transient are now to a large extent "washed" out of the computational domain instead of being reflected back. It is therefore expected that a computation with the "radiative" boundary conditions will eliminate the initial transient disturbances, and achieve a steady state solution faster than with other boundary conditions.

During a calculation with vibrating blades, a similar kind of reflection will be present at the boundaries with the first technique. This reflection may be significant, and the unsteady pressure amplitudes (everywhere in the flow field) may vary widely, depending upon the upstream and downstream computational lengths. It has however been concluded from the computed results that the blade surface pressure difference coefficient (Δc_p) does not change significantly in relation to these lengths, and so there are only small changes in the aerodynamic lift and damping coefficients.

In the case of the "radiative" boundary condition the reflections at the inlet and outlet surfaces are considerably reduced; only a minor reflection occurs because the simple waves are not yet perfectly straight

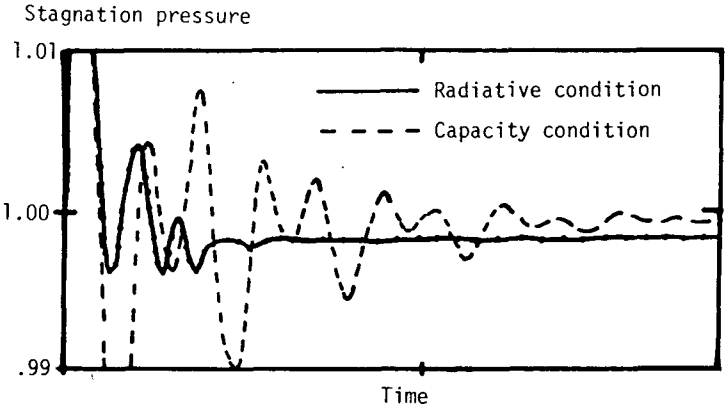

Fig. 11. Convergence rate for radiative and capacity boundary conditions.

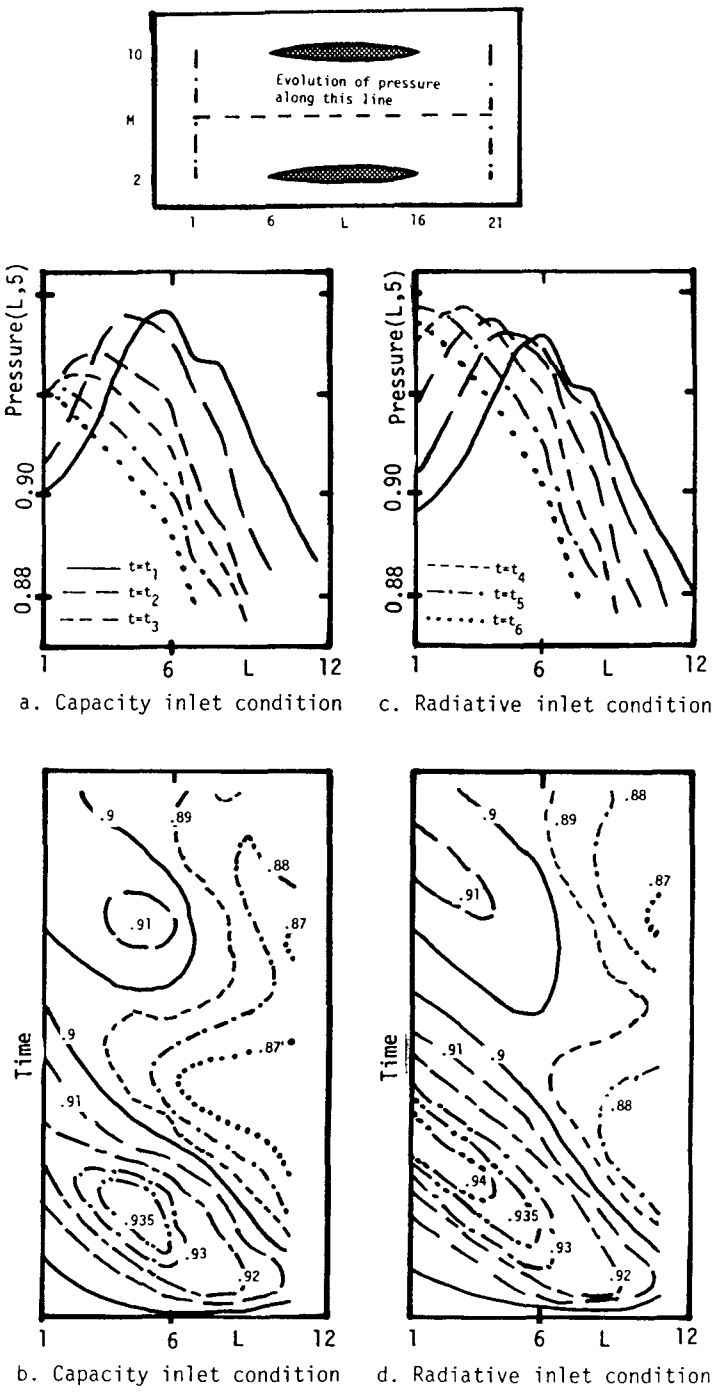

Fig. 12. Pressure distribution in the inlet region for the radiative and capacity inlet conditions.

and a small gradient still exists in the circumferential direction (the reflection will completely disappear in the case of perfectly straight waves, i.e. no gradients and actual 1-D flow). Fig. 13a refers to the pressure contour in the inlet region and shows no reflection at all and only minor reflections are shown in Fig. 13b, which refers to the velocity component $\tilde{w}$.

It can thus be concluded that for correct prediction of the local pressures in a given unsteady flow phenomenon, corresponding boundary conditions must be employed and that the use of the radiative simulation as a boundary condition introduces the smallest reflections back into the flow field. If, on the other hand, only unsteady blade surface pressure difference coefficients or integrated values, such as aerodynamic lift or damping are of interest, both boundary conditions have been experienced to give similar, although not identical, results.

CONCLUSIONS

A numerical method for solving the fully unsteady two-dimensional compressible inviscid flow (based on the Euler equations) through an oscillating subsonic cascade has been put forward. It has been shown that:

- the method gives stationary results which agree well with other numerical methods (/16,17/) for channel flow and moderately thick cascaded airfoils.
- the unsteady results obtained with the present method agree well with an analytical flat plate theory /4/, apart from certain cases in the region of subresonant blade vibration at high reduced frequencies.
- the assumed periodicity conditions for non-zero interblade phase angles have been validated.
- even if different physical inlet and outlet boundary conditions give identical stationary results, the unsteady behaviour of the flow may be quite different. The use of a "radiative" boundary condition introduces the smallest reflection from the boundary into the flow field.
- if there is a reflection at the inlet surface, the unsteady response in the cascade itself varies with the upstream computational length. For correct simulation of an actual physical phenomenon the choice of the boundary conditions, as is already known from linearized theories, is essential in unsteady flow investigations.

It can be concluded that the present numerical methodology can be used as a tool for computing and predicting wave propagation phenomena in unsteady flow through vibrating cascades. It also gives a good indication of the aerodynamic lift and damping coefficients on the vibrating blades.

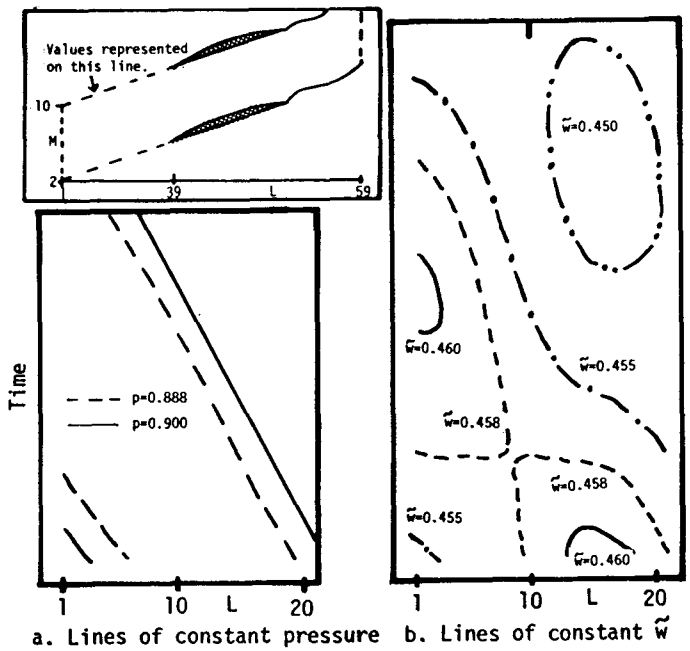

a. Lines of constant pressure b. Lines of constant $\tilde{w}$

Fig. 13. Reflection at inlet for radiative boundary condition.

ACKNOWLEDGEMENTS

The authors express their thanks to Brown Boveri & Cie, Baden, Switzerland, for supporting this project.

REFERENCES

/1/ FLEETER S.
Aeroelasticity Research for Turbomachines Applications
AIAA Paper 77-437, 1977

/2/ PLATZER M. S.
Transonic Blade Flutter: A survey of New Developments
The Shock and Vibration Digest, Vol. 14, No 7, 1982

/3/ ARNOLDI R.A.; MIKOLAJCZAK A.; SNYDER L.E.; STARGARDTER H.
Advances in Fan Compressor Blade Flutter Analysis and Predictions
Journal of Aircraft, Vol. 12, No. 4, 1975

/4/ SMITH S.N.
Discrete Frequency Sound Generation in Axial Flow Turbomachines
Reports and Memoranda No 3709, G.B., March 1972

/5/ VERDON J.M.
Further Development in the Aerodynamic Analysis of Unsteady Supersonic Cascades
ASME Papers No 77-GT-44, 77-GT-45, 1977

/6/ GRANT R. J.; WHITEHEAD D. S.
Force and Moment Coefficients for High-Deflection Cascades.
Proceedings "Symposium on Aeroelasticity in Turbomachines", Pages 85-127, Lausanne, Switzerland, 1980
/7/ CASPAR J. R.; VERDON J. M.
Development of an Unsteady Aerodynamic Analysis for Finite-Deflection Subsonic Cascades
NASA Contractor Report 3455, 1981
/8/ GALLUS H. E.; HOLTMAN H.; SERVATY S.
Computation of the subsonic flow field through oscillating compressor and turbine cascades
Proceedings "Symposium on Unsteady Aerodynamics of Turbomachines and Propellers", Cambridge, UK, 1984, pp 73-92
/9/ JOUBERT H.
Supersonic Flutter in Axial Flow Compressors
Proceedings "Symposium on Unsteady Aerodynamics of Turbomachines and Propellers", Cambridge, UK, 1984, pp 231-254
/10/ FRANSSON T.H.
Two-Dimensional and Quasi Three-Dimensional Experimental Standard Configurations for Aeroelastic Investigations in Turbomachine Cascades
Proceedings "Symposium on Unsteady Aerodynamics of Turbomachines and Propellers", Cambridge, UK, 1984, pp 361-396
/11/ ZIEREP J.
Theoretische Gasdynamik
G. Braun Verlag, Karlsruhe, Germany, 1976
/12/ FRANSSON T. H.
Numerical Investigation on Unsteady Subsonic Compressible Flows Through an Oscillating Cascade
Communication Laboratoire de Thermique Appliquée et de Turbomachines, Lausanne, Switzerland, No 13, 1985
/13/ MACCORMAC R.
The Effect of Viscosity in Hypervelocity Impact Cratering
AIAA PAPER 69-354, 1969
/14/ MORETTI G ; DE NEFF T
Shock Fitting For Everybody
Journal of Computers and Fluids, Vol. 8, No3, 1980
/15/ PANDOLFI M.
Numerical Experiments on Unsteady Flows Through Vibrating Cascades
Proceedings "Symposium on Aeroelasticity in Turbomachines", Pages 211-228, Lausanne, Switzerland, 1980
/16/ NI R.H.
A multiple-Grid Scheme for Solving the Euler Equations
AIAA Journal, Vol. 20, No11, 1982
/17/ DENTON J.D.
An Improved Time Marching Method for Turbomachinery Flow Calculation
ASME Paper 82-GT-239, 1982